Archives of Materials Science and Engineering

Volume 126
Issue 1
March 2024
Pages 22-33

International Scientific Journal
published monthly by the
World Academy of Materials
and Manufacturing Engineering

DOI: 10.5604/01.3001.0054.6780

Characteristics of polymer ring springs

G. Wróbel *, J. Kaczmarczyk
Department of Theoretical and Applied Mechanics, Faculty of Mechanical Engineering,
Silesian University of Technology, ul. Konarskiego 18A, 44-100 Gliwice, Poland
* Corresponding e-mail address: gabriel.wrobel@polsl.pl
ORCID identifier: https://orcid.org/0000-0002-7704-2466 (G.W.)

ABSTRACT

Purpose: The article presents a procedure for modelling and analysing a model system of ring and cone springs, in their particular material solution, using selected polymeric materials.

Design/methodology/approach: Subsequently, physical and mathematical models were presented, allowing the formulation of general design assumptions for the target products. The material models made were subjected to experimental tests to evaluate the correctness of the analytical models. Commercially available types of pure polyethylene and polypropylene were used as materials for machined parts based on catalogue properties. The material models were tested under variable static and periodically varying dynamic loads. The constructed finite element model was subjected to verification of the compatibility of the results of the numerical analysis with the results of simple experiments in order to assess the correctness of the model.

Practical implications: The correctness and adequacy of the computational model, confirmed in terms of simple load cases, will allow extending the scope of numerical simulation studies to systems that differ in material and geometric design features.

Originality/value: The performed studies have proved the advisability of using polymeric materials in the area of the design of ring springs. It allows for the significant expansion of the area of static and dynamic characteristics, which opens new fields of application for similar solutions. Due to the developed and verified numerical model, it becomes possible to analyse similar structural elements in terms of materials and geometry. In particular, interesting results can be expected if the research area is extended to composite materials. Also, the specific properties of plastics make it possible to expand the rationale field for similar systems.

The prices of the tested materials and, above all, the cost of processing in the presented structural solutions are competitive in cases where it is possible to obtain similar technical characteristics as steel structures. In addition, a wide range of design requirements can be met exclusively by polymer or composite springs. The tools presented here open up new possibilities for computer-aided design processes.

Keywords: Tapered rings, Polymers, Composites, Elastic characteristics, Friction, Finite element method

Reference to this paper should be given in the following way:

G. Wróbel, J. Kaczmarczyk, Characteristics of polymer ring springs, Archives of Materials Science and Engineering 126/1 (2024) 23-33. DOI: https://doi.org/10.5604/01.3001.0054.6780

METHODOLOGY OF RESEARCH, ANALYSIS AND MODELLING

1. Introduction

Springs, in mechanical engineering, are structural elements whose essential characteristics used in systems, both static and dynamic, is their elasticity [1, 3-8]. In a dominant way, the property characterises structural materials in their elastic load range. It occurs when, in the working load range, the stresses across the volume of the component remain within the elastic limit. The main features on which the stiffness of a spring depends are its form, dimensions and material characteristics of the material. Figure 1 shows the forms of the most commonly used spring elements: helical, flat, disc, annular (a), annular spring (b) and system of two annular springs (c).

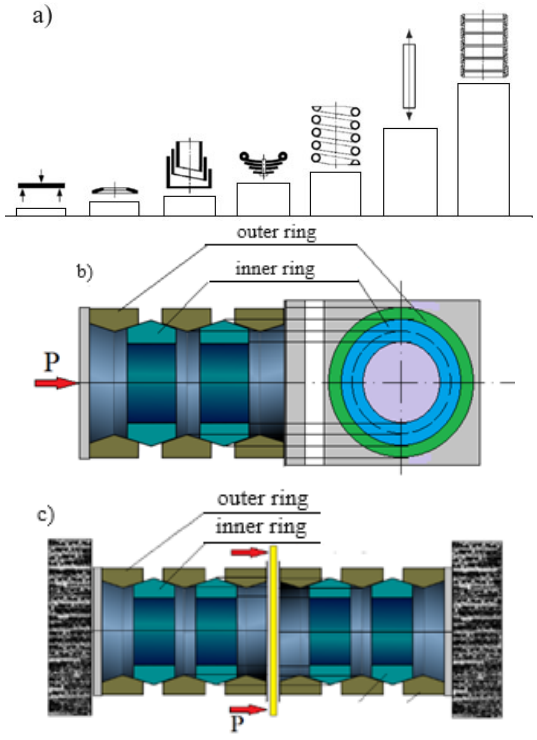

Fig. 1. Examples of spring elements (a), ring spring (b) and system of two ring springs (c)

In mechanical engineering, where the elements are mainly used, selecting the right element is made according to design criteria while maintaining the economic criterion. In a number of structural forms, ring spring solutions are relatively unpopular. It is probably due to their relatively higher precise manufacturing of the elements and the requirements related to the sensitivity of the elements to operating conditions. Different criteria for evaluating the design solutions of elastic elements apply when their task is to deform reversibly and dissipate the energy resulting from the work required to deform them under loading conditions. The dissipation can be carried out at the expense of permanent plastic deformation of the elements, with little change in their structure, but mainly through mechanisms of internal friction, plasticisation or external friction between parts of the structure and, in the case of hydraulic springs, fluid flow. Examples presented in this article include the leaf spring and the ring spring. The construction of these elements is characterised by large interfaces of the contacting elements, which allows using the friction occurring on these surfaces to dissipate energy by the way friction forces work.

The spring ring assemblies encountered on the market are mainly made of spring steel. The paper analyses the performance properties of model spring ring assemblies made of polymeric materials [2,11]. Significantly different physical properties of materials from the group, while maintaining the similarity of geometric characteristics of the elements, give the possibility of using such elements in different operating conditions, resulting from different utility functions. The developed physical model of a representative ring spring link was analysed under model loading conditions.

2. Ring spring model

Figure 2 shows an axial half-section of the spring model, composed of cooperating, symmetrical parts of the spring before (a) and after deformation (b).

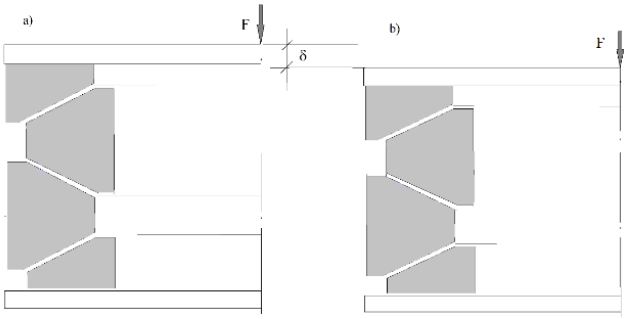

Fig. 2. Half-section of a ring spring in the state before (a) and after deformation (b)

Such springs consist of inner and outer rings, the cross-sections of which should be equal due to near-equivalent operating conditions. The principle of elastic axial deformation of an element is based on the relationship of reciprocal loads on the contact surfaces of the rings with

changes in their diameters, resulting in their mutual slip, the magnitude of which is determined by the relative change in diameters. The repeatability of the loading and deformation conditions for successive annular spring modules (Fig. 2) means that the loads on the outer rings, with the accuracy of local deviations, can be considered equal. Likewise, with regard to the inner rings. However, they differ in that the outer rings are stretched while the inner rings are compressed. By varying the number of elements, any deflection of the spring, and therefore any stiffness, can be obtained. By connecting the individual rings in series, their loads and deformations are equal, except for the end half-rings, whose load and deformation state depend on how they are supported. It is also possible to structurally provide the extreme elements with similar load and deformation states through a suitable attachment method. In view of the repeatability of the load states of the individual spring modules, the range of permissible loads on the spring does not depend on the number of modules and, therefore, on the number of rings. The maximum load for a different number of spring elements is constant, while the maximum deflection of the spring and its length change.

The above design features of coil springs make it possible to achieve a variety of performance characteristics that include the elastic stiffness of the elements, as well as the degree of strain energy dissipation. Quantitative measures of these characteristics depend on the geometric ones of the elements, such as ring diameters, cross-sectional dimensions and the number of elastic moduli. Equally important are the material characteristics of the elements, which are crucial both for the stiffness of the spring and its damping capacity.

3. Analysis of the loading condition of ring springs in the linear-elastic range, without friction

By design, deformation occurs in a linear range, in a quasi-static manner. The linear deformation range corresponds to the elastic deformation of the rings in the analysed load range while ignoring the friction that occurs on the tapered surfaces of the rings.

Figure 3 shows the spring modulus adopted for the analysis as a repetitive set of ring halves in contact.

Figure 4 shows the symmetrical part of the cross-section of the outer ring, with the reduced components of the loads resulting from the interaction on the contact surface of the inner ring marked for the case of spring compression. Initially, the static loading case is analysed, in which the equilibrium of the loaded system takes place without taking into account frictional forces.

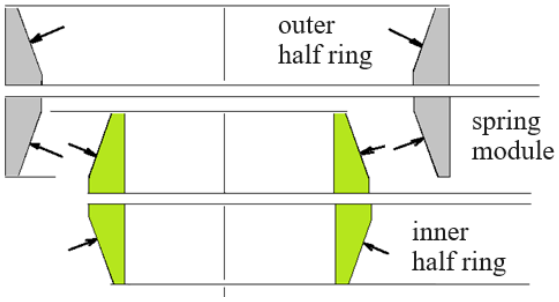

Fig. 3. Schematic of the half-ring system with the mutual pressure forces marked

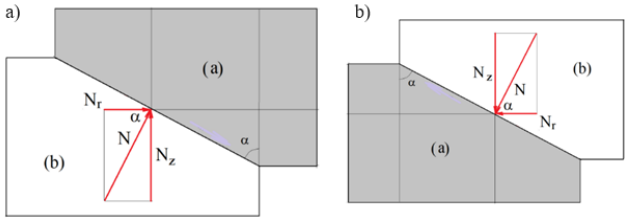

Fig. 4. The forces of mutual pressure of the rings

The circumferential force S_w, which depends on the compression force of the spring F, has a value:

$$S_w = F\mathrm{ctg}\alpha/2\pi \, . \tag{1}$$

It is a tensile force on the outer ring and a compressive force on the inner ring.

The increase in the average value of the radius R of the conical surface will be:

$$\delta R_z = RS_z/EA. \tag{2}$$

Loading the inner ring (Fig. 4a) will decrease the radius by the value:

$$\delta R_w = - RS_w/EA. \tag{3}$$

As a result, there will be an axial deflection of the spring link by the value:

$$\Delta z = RF/\pi EA. \tag{4}$$

Figure 5 shows the change in the relative position of the rings in the section of the analysed spring module.

It results in the stiffness of a single spring link, which the following expression can express:

$$K^{(1)} = (\pi EA)/R. \tag{5}$$

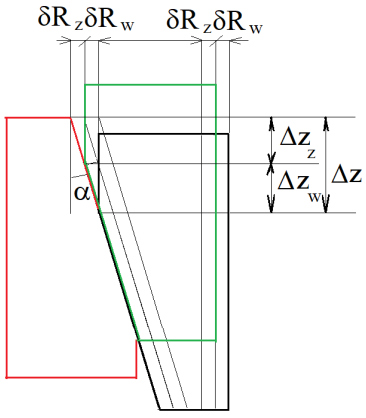

Fig. 5. Deflection of a single spring link

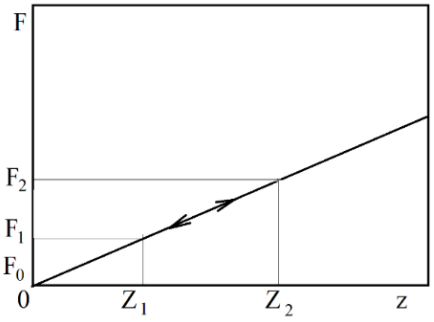

Fig. 6. Dependence of the deflection of the spring on the value of the axial force without taking friction into account

The absence of friction means that the dependence of the deflection of the spring on the value of the axial force remains the same for compression as for tension (Fig. 6).

4. Analysis of the loading condition of ring springs in the linear-elastic range with consideration of friction

A dry friction model will be adopted, in which there is a force on the conical surfaces of the rings proportional to the force of mutual pressure of the rings on the contacting conical surfaces.

Figure 7 shows cross sections of the pairing half-rings in the compression (a) and expansion (b) phases. On the edge of the conical slip surface of the rings, the vectors of circumferential loads on the axial force N_z and the components resulting from its distribution are marked: N – perpendicular to the contact surface, T – frictional force, their resultant N' and radial component N_r. They correspond to the intensities of loads on the outer ring, distributed linearly on the central circle of the conical contact surface.

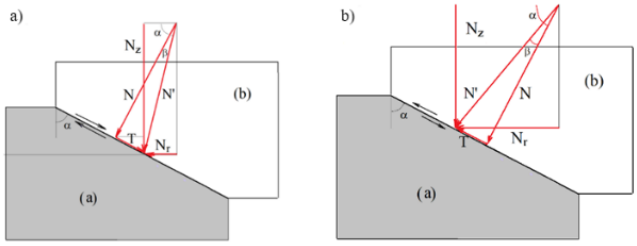

Fig. 7. Distribution of reciprocal loads of half-rings under frictional conditions for the case of compression (a) and expansion (b)

The proportions of the loads result from the assumed friction angle β, causing a change in the direction of the pressure force N'. The sliding friction coefficient μ is determined by the relationship: $tg\beta = \mu$.

Differing only in sign, the deformation of the rings describes the changes in radii determined by formulas (2) and (3).

The circumferential forces in the rings will change because the rings are loaded by oppositely directed reciprocal friction forces of T:

$$T = Ntg\beta = F\cos(\alpha+\beta)/2\pi(\sin\alpha + tg\beta\cos\alpha)\cos\beta. \quad (6)$$

The result is a sign-differing change in the radii of the outer and inner rings:

$$\delta R_z = -\delta R_w = RF\cos(\alpha+\beta)/2\pi EA(\sin\alpha + tg\beta\cos\alpha)\cos\beta. \quad (7)$$

Accordingly, analogous to equation (4), there will be a relative axial displacement of the rings:

$$\Delta z = \Delta z_z - \Delta z_w,$$
$$\Delta z = RF\cos(\alpha+\beta)tg\alpha/\pi EA(\sin\alpha + tg\beta\cos\alpha)\cos\beta. \quad (8)$$

The relationship between the axial load force of the spring F and the tensile force of the outer ring S_z, in this case, will take the form:

$$S_z = F\cos(\alpha-\beta)/2\pi(\sin\alpha - tg\beta\cos\alpha)\cos\beta. \quad (9)$$

The resulting changes in ring radii will be respectively:

$$\delta R_z = RS_z/EA,$$
$$\delta R_z = -\delta R_w = RF\cos(\alpha-\beta)/2\pi EA(\sin\alpha - tg\beta\cos\alpha)\cos\beta, \quad (10)$$

and the deflection of a single cell:

$$\Delta z = F\cos(\alpha-\beta)tg\alpha/\pi EA(\sin\alpha - tg\beta\cos\alpha)\cos\beta. \quad (11)$$

5. Analysis of the unloading phase of ring springs, taking friction into account

The deformation of the spring is accompanied by the execution of work by the forces compressing the spring – the cycle (1 - 2 - z_2 - z_1) (Fig. 8a). The process can occur under conditions of forced force, displacement or introduced energy. In each case, the deformation of the spring is accompanied by the making of work L_{12}:

$$L_{12} = (k/2)(1+\mu)(z_2^2 - z_1^2). \quad (12)$$

Part of this work - cycle (1 - 2 - z_3 - z_4) (Fig. 8a), with values:

$$U_{12} = (k/2)(z_2^2 - z_1^2), \quad (13)$$

causes an increase in the elastic energy of the spring deformation. The remainder – cycle (1 - 2- 3 - 4) (Fig. 8a), with a value:

$$L^t_{12} = \mu k/2(z_2^2 - z_1^2), \quad (14)$$

which is associated with the performance of frictional work converted into heat.

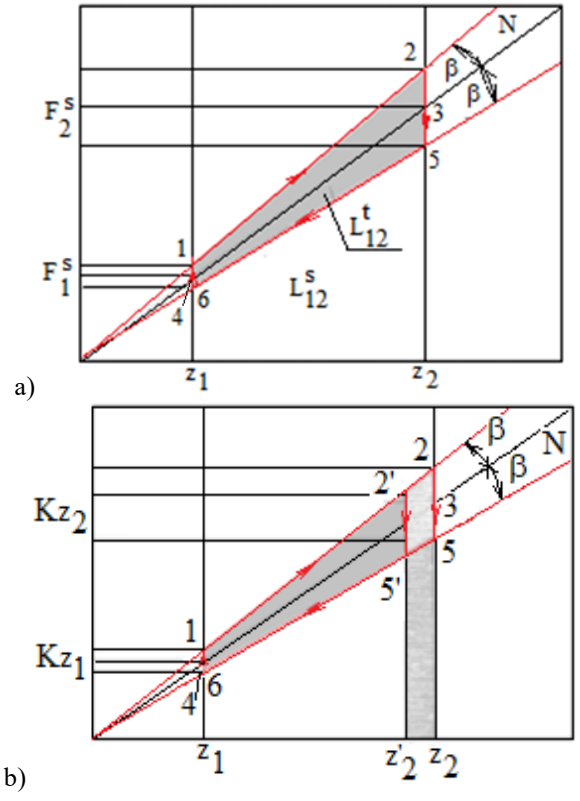

Fig. 8. Diagrams of the deformation cycle of the spring modulus with the dissipated frictional work marked

In the return movement, the elastic energy of the spring deformation U_{12}, reversibly given back to the cushioned system, is reduced by a part-cycle (3 - 5 - 6 - 4) (Fig. 8b), corresponding to the work of the frictional force performed during expansion:

$$L^t_{34} = \mu k/2(z_2^2 - z_1^2) = L^t_{12}. \quad (15)$$

6. Experimental study

The experiment involved the compression of a single spring module, composed of a pair of polyamide rings, for three contact surface cone angles: $\alpha_1 = \pi/6$, $\alpha_1 = \pi/3$, $\alpha_1 = \pi/4$. Photographs of the two-element specimens are shown in Figure 9. They differ in the material of the associated pairs and the angles of the conical surface.

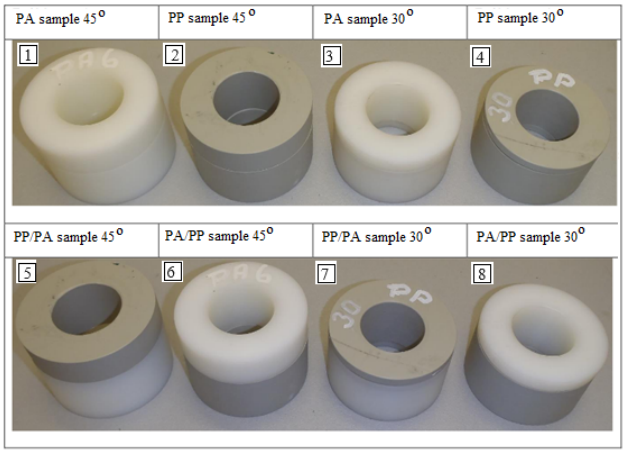

Fig. 9. Samples of ring pairs

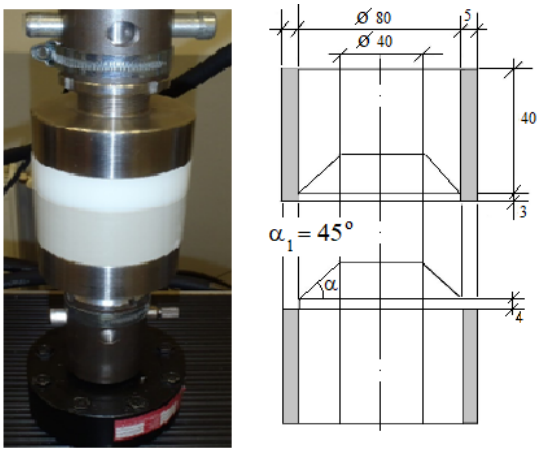

Fig. 10. A section of the test stand and cross-sectional drawings of the compressed rings

Figure 10 presents a section of the test stand and cross-sectional drawings of the compressed rings.

Static compression tests of the tested cells – pairs of rings were performed [12,13]. Selected characteristics are shown in Figure 11.

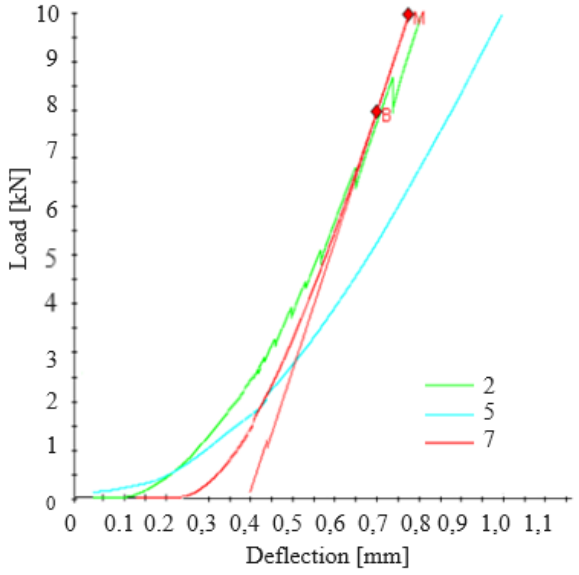

Fig. 11. Selected compression characteristics

Dynamic alternate loading tests of the cells were also performed. The selected load waveforms are shown in Figure 12. The visible thin lines correspond to the first load cycle, during which the cells were reached, and the thick lines correspond to overlapping steady-state cycles. They correspond to the model load waveforms of the spring shown in Figure 8.

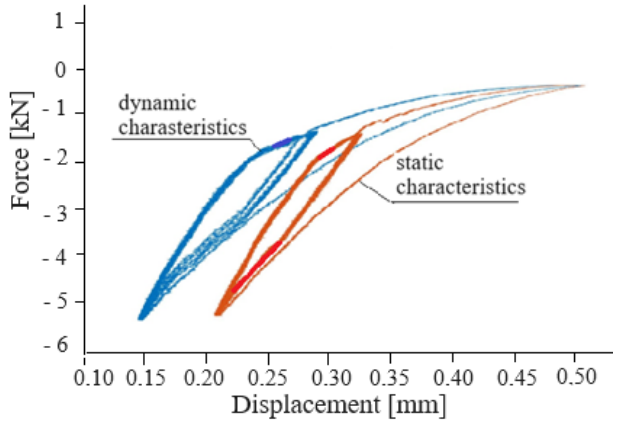

Fig. 12. Selected load waveforms

7. Numerical analysis

The numerical analysis conducted in the study employs the finite element method, leveraging the advanced computational capabilities of LS-DYNA to investigate the static behaviour of displacement in response to compression and release. The scientific investigation meticulously simulates the physical phenomenon by assuming a relationship between displacement and pseudo-time, a strategic approach designed to capture the steady state response of the material under study.

The model at the core of the research is intricately structured, consisting of several components that have been discretised into finite elements, thereby facilitating a detailed examination of their behaviour under applied conditions. Specifically, the finite elements employed are three-dimensional solid elements, each characterised by three degrees of freedom per node. The configuration allows for the simulation of translational movements in three orthogonal directions (x, y, and z axes), ensuring a comprehensive representation of the material's geometric and physical properties. Such a detailed meshing technique is crucial for accurately capturing the complex interactions between the elements in contact when subjected to compression and subsequent release.

By applying LS-DYNA, known for its robustness in handling complex and highly nonlinear problems, the study achieves high precision in simulating the displacement phenomena. The software sophisticated algorithms allow for the integration of time-dependent material and geometric nonlinearities, enabling the analysis of the model response with respect to pseudo-time. The approach provides valuable insights into the deformation mechanisms and the material resilience to static loading conditions.

Employing three-dimensional solid elements with three degrees of freedom per node through LS-DYNA facilitates a detailed scientific investigation into the compressive and release of the material, highlighting the nuanced interplay between displacement and pseudo-time. The research contributes significantly to understanding material behaviour under static loading, offering potential applications in designing materials and structures with enhanced performance characteristics in response to such conditions.

Figure 13 presents a detailed finite element model [9] that illustrates the intricate interaction occurring on the conical surfaces of the rings. The model meticulously simulates the statics of contact and frictional forces as the rings engage, highlighting the precision with which the finite elements capture the complex geometrical and mechanical behaviour of the surfaces in contact.

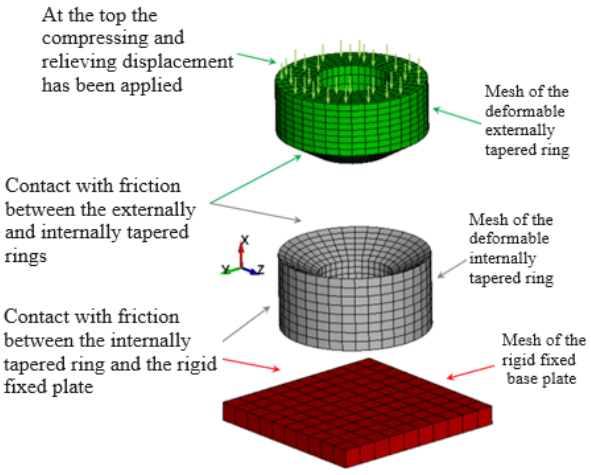

Fig. 13. Mesh of the finite element model

Each element within the model contributes to an accurate representation of the stress distribution and deformation that emerge from the interaction of the conical surfaces under operational conditions. The visualisation underscores the sophisticated computational approach employed to analyse the structural integrity and performance of the ring assembly, providing essential insights into the design.

The material characteristics [10]:

- density $\rho = 1114$ kg/m^3,
- Young's modulus E = 2590 MPa,

are presented in Figure 14.

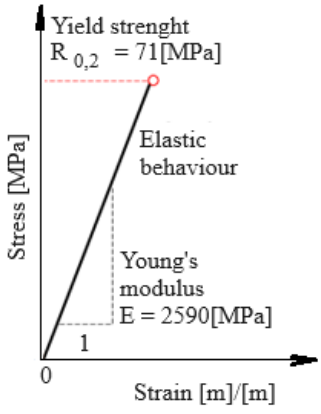

Fig. 14. Characteristic for the assumed material model of polyamide PA 6

Figure 15 shows a comprehensive graphical representation of the static characteristics that define the behaviour of a conical spring during its loading and unloading phases. During the loading phase, the graph illustrates how the spring undergoes deformation. This portion of the curve is crucial for understanding the conical spring behaviour under compressive forces, indicating the level of stiffness may begin.

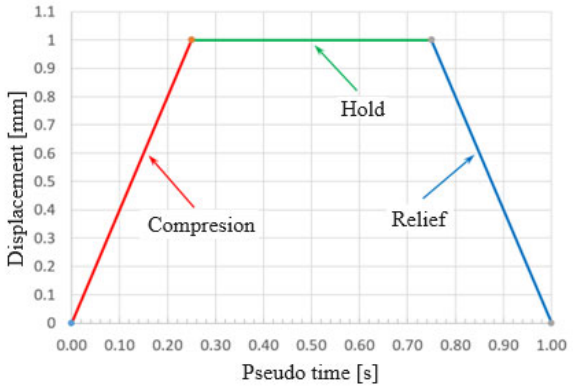

Fig. 15. Static characteristics of the modelled process

The compression and relieving process of the conical rings has been modelled using the finite element method and the computer system LS-DYNA. The numerical results have been juxtaposed for several successive pseudo-time intervals for nonlinear quasi-static analysis to facilitate the investigation of the compression and relieving process mechanism using the loading applied at the top surface of the internally tapered ring directed vertically downwards and upwards. Three variants have been researched for three different conical angles: $\varphi = 30°$, $\varphi = 45°$ and $\varphi = 60°$, respectively.

Figure 16 provides a detailed visual representation, capturing the selected successive phases of deformation alongside a comprehensive distribution of reduced Huber-Mises stresses on the surfaces of the rings. The detailed exposition focuses on the scenario where the cone angle is $\varphi = 30°$. It meticulously highlights how the stress distribution varies across different stages of deformation, emphasising the nuanced patterns of Huber-Mises stresses that evolve due to the specified geometric condition.

The level of detail offers profound insights into the stress response mechanisms under the given angular constraint, showcasing the critical areas of stress concentration and the overall structural resilience of the rings.

Figure 17 compares the total internal energy, measured in joules (J), as it evolves over pseudo-time, measured in seconds (s), across three distinct scenarios characterised by varying cone angles. Specifically, the figure showcases the static changes in internal energy for cone angles set at 30°, 45°, and 60°, respectively. The comparison elucidates how

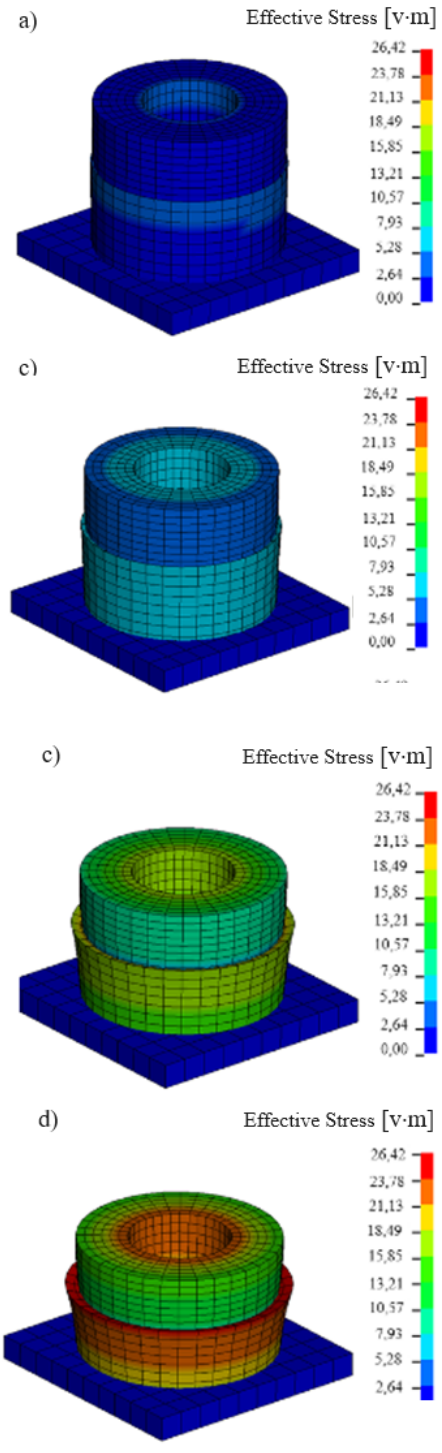

Fig. 16. Graphical images of the selected successive phases of ring deformation and the distribution of reduced Huber Mises stresses on the surface of the rings, for the case of the cone angle φ = 30°

the cone angle significantly influences the energy within the system, reflecting the impact of geometric alterations on the mechanical behaviour over pseudo-time. By plotting the total internal energy against pseudo-time for each of these cone angles, the figure highlights the differential energy absorption and release patterns, thereby offering insights into the efficiency and resilience of the system under varying geometric constraints. Such an analysis is crucial for understanding the role of cone angle in the mechanical performance and energy distribution of the system, guiding the optimisation of design parameters for enhanced structural integrity and functional efficiency.

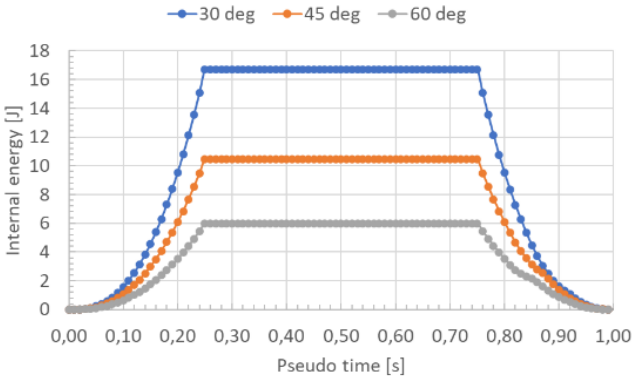

Fig. 17. Comparison of total internal energy [J] with pseudo-time [s] for three different cone angles equal to 30°, 45° and 60°, respectively

Figure 18 offers a detailed comparative analysis of the internal energy, quantified in joules (J), as it is distributed across the pairing elements over pseudo-time, measured in seconds (s), focusing specifically on two configurations distinguished by their taper angles: 30° (represented in part a) and 60° (represented in part b). The comparative visual representation is designed to elucidate how variations in the taper angle influence the spatial and temporal distribution of internal energy within the system, highlighting the correlation between geometric alterations and energy. The figure reveals that an increase in the taper angle from 30° to 60° significantly affects strain energy distribution between the interacting elements. Specifically, as the taper angle enlarges, there is a notable approximation in the strain energy levels of the two elements, suggesting that the geometric modification leads to a more uniform distribution of energy throughout the system. The observation implies that the taper angle plays a crucial role in mediating the mechanical interaction between the elements, where a larger angle tends to equalise the energy distribution, potentially enhancing the system overall mechanical efficiency and stability.

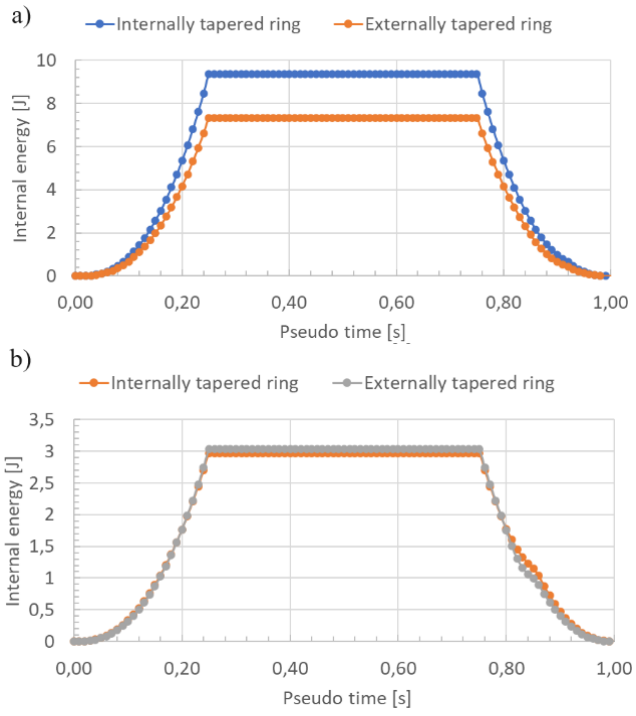

Fig. 18. Comparison of partial internal energy [J] versus pseudo-time [s] for internally tapered ring and externally tapered ring, respectively, for the conical angle equal to 30° (a) and 60° (b)

By presenting the internal energy distribution in relation to pseudo-time for taper angles of 30° and 60°, Figure 18 demonstrates the nature of energy transfer within the system. It provides valuable insights into the impact of geometric design on the mechanical behaviour of the pairing elements. Such analysis is critical for optimising design parameters to achieve desired performance characteristics, ensuring that structural and functional efficiencies are maximised through appropriate geometric configurations.

8. Description of achieved results

The research paper presents the comprehensive development and analysis of a physical model for a ring spring, initiating its conceptualisation and extending into a rigorous mathematical analysis. The process involved deriving critical relationships that define the operational characteristics and performance parameters of the spring module in question. A thorough experimental and numerical verification process was employed to validate the theoretical model and its underlying assumptions, utilising the finite element method as a cornerstone analytical tool. The verification process was meticulously designed to ensure that the model accurately reflects the geometric characteristics of the actual springs being studied, thereby enhancing the reliability of the simulation results.

The experimental phase involved the fabrication of spring specimens from polymeric materials, specifically using pure and filled PA 6 polyamide. This choice of material was significant, given its prevalent use in engineering applications and its interesting properties. The verification extended to pairs of ring elements, which were carefully selected to represent a variety of material combinations and to encompass a range of contact surface cone angles. The elements were subjected to static and dynamic compression tests, characterised by periodic loading to simulate operational conditions closely.

The numerical modelling was pivotal in simulating the load-strain behaviour of the spring link, enabling a detailed analysis of several key factors. They included the stiffness distribution within the link, the internal load distribution, and the strain energy throughout the system. The simulation provided valuable insights into the mechanical behaviour and performance of the ring spring under various loading conditions, offering a predictive view of its operational capabilities.

The culmination of this research is the provision of essential knowledge that lays the groundwork for the future design and construction of ring springs utilising polymeric materials. The innovative approach and original findings of this study underscore the significance of integrating physical modelling, mathematical analysis, and experimental and numerical verification in developing engineering solutions. The comprehensive methodology validates the model and enhances the understanding of the dynamic behaviour of polymeric ring springs, thereby contributing to the field of mechanical engineering with novel design principles and construction methodologies for advanced spring systems.

9. Conclusions

The comprehensive experimental and model studies carried out within this research framework have highlighted the considerable advantages of venturing into novel designs and material selections for ring springs. The exploration is not merely academic but paves the way for broadening the spectrum of potential applications for these engineering components. The impetus for such an expansion is rooted in the observed substantial differences in the material and

strength properties between polymeric materials and traditional metals. Polymeric materials, with their unique combination of flexibility, durability, and lighter weight, offer an intriguing alternative to metal springs, potentially transforming the design and functionality of spring mechanisms in various applications.

The findings underscore the necessity of further research, particularly emphasising the need to consider a wider range of physical properties of materials beyond the mechanical strengths traditionally focused on.

Moreover, the conclusions advocate for including composite materials in future studies. Composites, with their ability to be engineered to exhibit specific properties by combining different materials, present a fertile ground for innovation in spring design. In pursuit of these advanced design solutions, research must be directed towards understanding the interplay between the physical properties of materials and the specific performance requirements of potential applications. Such an approach will enable the development of ring springs that are not just alternatives to their metal counterparts but are superior in addressing the nuanced demands of modern engineering challenges.

In conclusion, the conducted studies herald a promising frontier in the design and application of ring springs, urging a multidisciplinary research approach that embraces new materials, including polymers and composites, and considers a comprehensive array of physical properties. The strategic direction is essential for devising innovative design solutions that meet specific performance criteria, heralding a new era in the application and functionality of ring springs.

Research funding

Work was carried out within the initial stages of NCBR project No. POiR-01.01-00-086/19 entitled “Development of innovative technology for GRP loose flanges using recycled material”.

Authors contribution

G. Wróbel – literature study, development of a physical and mathematical model of the process of operation of the studied system. Development of a program of experimental and numerical research. Development of the system I edition of the work; participation in the development of the publication 90%.

J. Kaczmarczyk – development of the model for numerical analysis, execution, and development of calculation results; participation in the development of the publication 10%.

Additional information

Selected issues related to this paper were presented at the 26th International Scientific Conference on “Achievements in Mechanical and Materials Engineering with Bioengineering and Dental Engineering” AMME & bio 2024 organised on 20th-23rd May 2024 in Wisła Malinka, Poland.

References

[1] G. Wróbel, Characteristics of polymer ring springs. Archives of Materials Science and Engineering 114/1 (2022) 13-23. DOI: https://doi.org/10.5604/01.3001.0015.9848

[2] M. Radeş, Shock isolation systems, S. Brown (ed), Encyclopedia of Vibration, Academic Press, Cambridge, MA, 2001, 1180-1184. DOI: https://doi.org/10.1006/rwvb.2001.0177

[3] Y. Ling, S. Wu, J. Gu, H. Lai, A Novel Ring Spring Vibration Isolator for Metro Superstructure, Applied Sciences 11/18 (2021) 8422. DOI: https://doi.org/10.3390/app11188422

[4] C. Zou, Y. Wang, J.A. Moore, M. Sanayei, Train-induced field vibration measurements of ground and over-track buildings, Science of The Total Environment 575 (2016) 1339-1351. DOI: https://doi.org/10.1016/j.scitotenv.2016.09.216

[5] C. Zou, Y. Wang, P. Wang, J. Guo, Measurement of ground and nearby building vibration and noise induced by trains in a metro depot, Science of The Total Environment 536 (2015) 761-773. DOI: https://doi.org/10.1016/j.scitotenv.2015.07.123

[6] C. Zou, J.A. Moore, M. Sanayei, Y. Wang, Impedance model for estimating train-induced building vibrations, Engineering Structures 172 (2018) 739-750. DOI: https://doi.org/10.1016/j.engstruct.2018.06.032

[7] Grimm: Ringfeder friction ring springs. Technical description (in Polish). Available from: https://grim.pl/main_libs/files/assets/1/sprezyny_pierscieniowe_cierne/sprezyny-pierscieniowe-cierne.pdf

[8] M. Sitarz, W. Gamon, Rail buffers - requirements, design, testing, Technika 9 (2012) 29-35 (in Polish).

[9] P. Borkowski, G. Krzesiński, P. Marek, T. Zagrajek, Finite Element Method in mechanics of materials and structures. Solving selected problems with the ANSYS system, 2nd Edition, Publishing House of the Warsaw University of Technology, Warszawa, 2022 (in Polish).
[10] W. Szlezynger, Z. Brzozowski, Plastics. Vol. I: general-purpose plastics, Educational Publishing House FOSZE, Rzeszów, 2023 (in Polish).
[11] W. Bodaszewski, I. Markiewicz, D. Bojczuk, Strength of materials – experimental studies, BEL Studio, Warszawa, 2011 (in Polish).
[12] Z. Dyląg, A. Jakubowicz, Z. Orłoś, Strength of materials. Vol. II, WNT, Warszawa, 2000 (in Polish).
[13] M. Bijak-Żochowski M. Dietrich, T. Kacperski, J. Stupnicki, J. Szala, J. Witkowski, Fundamentals of machine construction, M. Dietrich (ed), 3rd Edition, PWN, Warszawa, 2017 (in Polish).